

Stars & Gas in the Galaxy Pair II Zw 70/71

A. L. Cox

Department of Physics & Astronomy, Beloit College

700 College Street, Beloit, WI 53511-5595

coxa@beloit.edu

L. S. Sparke

Astronomy Department, University of Wisconsin – Madison

475 N. Charter St., Madison, WI 53706

sparke@astro.wisc.edu

A. M. Watson

Instituto de Astronomía, Universidad Nacional Autónoma de México

Apartado Postal 72-3 (Xangari), 58089 Morelia, Michoacán, México

a.watson@astrosmo.unam.mx

G. van Moorsel

National Radio Astronomy Observatory, Array Operations Center

P.O. Box 0, Socorro, NM 87801

gvanmoor@nrao.edu

ABSTRACT

II Zw 71 (UGC 9562) was classified as a “probable” polar-ring galaxy in the Polar-Ring Catalog ((Whitmore *et al.* 1990)), based upon its optical appearance. We present 21 cm and optical observations of this galaxy and its companion, the blue star-forming dwarf II Zw 70. Our 21 cm observations show that 5×10^8 solar masses of H I is present in a polar ring orbiting II Zw 71, and show a spatially and kinematically contiguous streamer with 2.5×10^8 solar masses of H I gas between the two galaxies. This gaseous bridge, plus our observations of H α line emission in the polar ring and in II Zw 71, are strong evidence for an ongoing interaction between the two galaxies. However, the configuration of the streamer suggests that the polar ring itself may well have predated the current interaction, which then stimulated an outburst of star formation in the ring gas.

Subject headings: galaxies, neutral hydrogen, polar rings

1. Introduction

Polar-ring galaxies (PRG’s) are systems with two kinematically distinct components. The central component (the “host galaxy”) is usually a small S0 galaxy, or occasionally an elliptical galaxy, and the outer component (the “polar ring”) is a ring or annulus of material in a nearly circumpolar orbit about the host. The fact that the angular momentum vectors of the host galaxy and of the polar ring are nearly orthogonal indicates that PRG’s are most likely the end products of mergers or accretion events, rather than a single coherent formation process. The Polar-Ring Catalog ((Whitmore *et al.* 1990), hereafter PRC) classifies 6 galaxies as kinematically-confirmed polar rings (category “A” in the PRC), and 27 galaxies as “probable” polar rings based upon their optical appearance (category “B” in the PRC). The catalog is frozen, but some category “B” galaxies have since been confirmed since its publication (see (Sparke & Cox 2000)).

The origin of the material in polar rings is something of a mystery, because the gas masses involved are so large. Polar rings are gas-rich, with typically a few billion solar masses of H I gas ((van Gorkom *et al.* 1987); (Richter *et al.* 1994); (Cox & Sparke 1996); (Arnaboldi *et al.* 1997)), and often significant molecular gas and dust as well (see (Galletta *et al.* 1997)). The identified polar rings have enough stars that we can see the rings at optical wavelengths, and stellar rings lie within the rings of neutral gas (*e.g.* (van Gorkom *et al.* 1987); (Arnaboldi *et al.* 1997)). Because accreted gas can dissipate energy while the stars cannot, gas and stars will tend to settle into very different final configurations. The stars now in the polar ring must have been formed from the gas after it had settled into the thin ring structure (*e.g.*, (Dubinski & Christodoulou 1994)).

The host galaxies are small early-type galaxies, typically with $L_B < 10^9 M_\odot$. There is no evidence that the host galaxies themselves contain substantially more cool gas and dust than other early-type galaxies without polar rings (see (Richter *et al.* 1994)). Their radio continuum emission is not significantly stronger than early-type galaxies without polar rings ((Cox & Sparke 1994); (Cox *et al.* 2000)). This lack of radio continuum emission indicates that any strong starburst activity which may have been induced by the event that formed the ring has since ceased. Even making no allowance for the mass of stars which have formed in the polar rings, these galaxies have captured the equivalent of the entire gas content of a typical spiral galaxy (*e.g.*, (Roberts & Haynes 1994), hereafter RH94).

It is not clear that a large spiral galaxy could accrete onto a small S0 galaxy without leaving behind a very disorganized system. If the spiral companion was destroyed, its stars would not dissipate kinetic energy to form a ring as the gas has done, but should be visible as faint shells or diffuse light around the merged system. Although some PRG’s are known to have shells, many PRG’s do not have visible shells (PRC). If the ring material was taken from the outer parts of a spiral galaxy, then we should be able to see the remains of this companion, but many polar rings have

no nearby companions. If the polar ring was formed by accretion of a gas-rich dwarf galaxy, there might be no conspicuous stellar shells, and no visible remnant of the encounter. But dwarf irregular galaxies at the present day contain too little neutral gas to make polar rings; the upper end of the H I mass function for present-day dwarf galaxies is only a few times $10^8 M_{\odot}$ (*e.g.* (Briggs & Rao 1993); (Briggs 1997); (Matthews *et al.* 1998a)). Searches for clouds of primordial intergalactic H I indicate that there is very little gas in this form at the current epoch (*e.g.* (Brinks 1993); (Taylor *et al.* 1996); (Zwaan *et al.* 1997)). If PRG’s are stable structures, most of them may have formed early in the history of the universe, when large clouds of intergalactic gas should have been more common.

In any case, it is highly probable that the accretion of material onto many host galaxies is not complete. The gas of the polar ring has come from an orbit of high angular momentum with a large impact parameter, and it is likely that streamers of gas would remain around most newly-formed polar rings well after the original encounter ((Hibbard & Mihos 1995)). The study of probable polar-ring systems which have nearby companions are therefore very likely to reveal gaseous tails or bridges which may help us better understand the interactions which form polar rings.

II Zw 71 (UGC 9562) is classified as “B-17”, a “probable” polar ring system, in the PRC. An optical image of this galaxy and its blue dwarf companion, II Zw 70 is shown in Figure 1; the polar ring runs NE to SW. Optical spectroscopy in the H α emission line of II Zw 71 by Reshetnikov & Combes (1994) revealed two gaseous components with orbits nearly perpendicular to each other — one with a velocity gradient along the apparent major axis of the polar ring, and another with a velocity gradient along the apparent major axis of the host galaxy. II Zw 71 is thus a kinematically-confirmed polar-ring galaxy. Earlier observations of this system by Balkowski *et al.* (1978; hereafter BCW78) in the 21 cm line with the Westerbork Synthesis Radio Telescope (WSRT) also showed rotation of gas along the polar ring, and in addition detected a cloud of H I gas between the two galaxies. No optical counterpart brighter than 25.5 mag arcsec⁻² to this cloud was detected in *B* band. The II Zw 70/71 system is thus one of the best known candidates for a polar ring in the process of formation by accretion of gas from a nearby companion.

We have obtained observations in the 21 cm line of H I, using the Very Large Array (VLA¹) aperture synthesis telescope. These observations are more sensitive than the observations by BCW78, and have approximately twice the spatial and velocity resolution. We have also obtained H α and broad-band optical images of this system, to search for evidence of ongoing star formation and for an optical counterpart of the gas cloud between II Zw 70 and II Zw 71. The H I distribution and kinematics of the II Zw 70/71 system are presented in Section 2, and the optical data in Section 3. In Section 4, we discuss the morphology of the stars and gas in this system, and investigate the possibility that the polar ring around II Zw 71 is the product of an ongoing accretion event from gas originating in II Zw 70. We take $H_0 = 75 \text{ km s}^{-1} \text{ Mpc}^{-1}$, implying a distance of 18.1 Mpc for the system.

¹The National Radio Astronomy Observatory is a facility of the National Science Foundation operated under cooperative agreement by Associated Universities, Inc.

2. 21 cm Observations

The II Zw 70/71 system was observed with the “C” and “D” configurations of the VLA. The C-configuration data were obtained on 02 December 1994, and the D-configuration data on 02 May 1995. The instrumental parameters for the observations are summarized in Table 1. Our velocity resolution was $\simeq 2.6 \text{ km s}^{-1}$. Because of the high velocity resolution, we observed the II Zw 70/71 system with two independent bandpasses (IF’s), centered at 1232 & 1268 km s^{-1} . This observing mode allowed us to have a wide enough total bandwidth to include all of the gas in both systems, without sacrificing velocity resolution.

Calibration and mapping were performed using the NRAO Astronomical Image Processing System (AIPS). The data from each configuration and each IF were calibrated and continuum-subtracted independently. Standard calibration procedures were followed, as described in Appendix B of the *AIPS Cookbook* ((Cox 1994)). As the IF’s were separated in velocity space, each IF contained channels which were free of line emission on only one side of the bandpass. A continuum dataset was constructed for each IF by averaging together the line-free channels in the u, v plane; this dataset was subtracted from all channels in that IF to give one continuum-subtracted set of line data for each IF. This method of continuum subtraction assumes that the continuum spectrum is flat over the bandpass of the observation, and that there are no strong continuum sources. Both of these criteria were satisfied by this dataset. Faint 21 cm continuum emission was detected at the positions of II Zw 70 and II Zw 71; a continuum map is shown in Figure 1, and the nature of this emission is discussed further in Section 2.1.

After continuum subtraction, the end channels were discarded and all four datasets (two IF’s for each configuration) were combined in the u, v plane to yield a single, continuum-subtracted dataset for the II Zw 70/71 system. Maps were made and corrected for instrumental response using the robust imaging task, IMAGR. Robust weighting improves the shape of the synthesized beam dramatically for multi-configuration datasets, as these data have even higher concentrations of short baselines than single-configuration data ((Briggs 1995); see also Section 5.2.3 of the *AIPS Cookbook*). The resulting channel maps have a spatial resolution of $22.5'' \times 20''$, and include structures with sizes up to $10'$; they are shown in Figure 2.

2.1. Continuum Emission

As shown in Figure 1, faint 21 cm continuum emission was detected at the positions of II Zw 71 and its companion galaxy, II Zw 70. The emission observed in II Zw 71 is centered on an H II region in the polar ring; no emission is observed in the central portion of the host galaxy. Because the continuum map is constructed from an average of the line-free channels, the RMS noise in the continuum map is only $0.2 \text{ mJy beam}^{-1}$, significantly lower than the RMS in the individual line channels (see Table 1). As part of a radio continuum survey of polar-ring galaxies ((Cox & Sparke 1994); (Cox *et al.* 2000)), we have also obtained 6cm continuum observations of

these sources. The 6cm observations were made in the VLA “B” configuration, which gives a synthesized beam of approximately $5''$. The on-source integration time was only 30 minutes, but because of the larger bandwidth of the continuum observations (50 MHz), the RMS noise in the 6cm maps is $0.09 \text{ mJy beam}^{-1}$. The 6cm emission which was detected was also unresolved, and at the same positions as the 21 cm emission.

As the sources are unresolved at both wavelengths, differences in baseline coverage between the two sets of observations should not present a problem when calculating radio spectral indices. In both II Zw 70 and II Zw 71, the spectral indices (defined by $S \propto \nu^\alpha$) are quite steep, with $\alpha \simeq -1$. This is consistent with radio spectral indices of star-forming galaxies (*e.g.* (Condon *et al.* 1991)). Faint, steep-spectrum radio continuum emission is not uncommon in polar-ring galaxies ((Cox 1996)), and the emission may be either centrally concentrated or extended along the polar ring ((Arnaboldi *et al.* 1997); (Carilli & van Gorkom 1992)).

2.2. Moment Maps

Using the cleaned map cube at 5.2 km s^{-1} velocity resolution, we constructed moment maps of the velocity profile at each point. To improve the sensitivity to low-level extended emission, we first smoothed the entire map cube to $40''$ resolution. We then selected the areas which contained real line emission in this smoothed cube, using a two-step process. First, we applied a uniform flux cutoff to the entire cube, eliminating all pixels with an intensity less than 1 mJy beam^{-1} (twice the RMS noise in the smoothed maps). To minimize the confusion from noise peaks not related to real line emission, we then inspected each velocity channel visually, and selected only those areas which appeared to contain line emission, and blanked all other areas. These smoothed and clipped channel maps were then used as masks; we calculated moment maps from the cube at full resolution, including only the flux from regions where the smoothed maps were found to have emission, and the flux in the full-resolution maps was above a $2\text{-}\sigma$ cutoff level of $0.8 \text{ mJy beam}^{-1}$.

The total-intensity map at 21 cm (Figure 3) shows significant quantities of neutral gas in the PRG (II Zw 71), its dwarf companion (II Zw 70) about $260''$ away, a streamer which appears to connect the two, and an extension of the gas to the east of the polar ring. The polar-ring gas extends about $50''$ to the north and $70''$ to the south, and looks “C” shaped; the ring seems to bend towards II Zw 70 at both ends.

Figure 3b is a position-velocity cut taken along the optical major axis of the polar ring. In general, the rotation of the gas is along the ring major axis, but there is a larger spread in velocity and space on the southern side of the ring than on the northern side. Figure 3c is plotted along the position angle of the H I streamer seen between the two galaxies. To increase our signal-to-noise for the faint streamer, the data for this position-velocity profile were summed out to a distance of 1.5 perpendicular to this axis, on each side of the streamer. This includes all 21 cm line emission detected in these observations. The streamer is contiguous with both galaxies, in both position

and velocity space — a strong indication of an ongoing interaction between II Zw 70 and II Zw 71. However, the gas that extends to the east of the polar ring appears to be a continuation of the streamer in both position and velocity, which suggests that the streamer passes in front of the polar ring, or behind it.

The intensity-weighted velocity field for the II Zw 70/71 system is shown in Figure 4. The optical appearance of the polar ring in II Zw 71 suggests that we see it almost edge-on. With a rotation speed of 95 km s^{-1} , this gives a dynamical mass of 19 billion M_{\odot} within a $50''$ distance from the center of the galaxy, or $M/L_B \approx 21$. This is much larger than the value $M/L_B = 2.8$ within $30''$, derived by (Reshetnikov & Combes 1994) from long-slit spectroscopy of the ring in $\text{H}\alpha$. The position-velocity cut of Figure 3b shows no sign that the rotation speed of the ring gas is dropping off, even far outside the optical radius of the host galaxy in II Zw 71 ($18''$; see (Sackett 1991)). Thus a significant amount of the mass in this galaxy must be in the form of dark matter.

The gas of the companion galaxy, II Zw 70, exhibits regular rotation about its apparent optical minor axis. This is in contrast with the earlier observations by BCW78, where the rotation appeared to be skewed from the minor axis, so that the kinematic major axis was oriented almost exactly east-west. However, their observations probably confused gas associated with II Zw 70 with that from the streamer of H I between the two galaxies. This problem is reduced in the current observations by our improved spatial resolution ($\simeq 21''$ for these observations, compared with $\simeq 34''$ for the observations of BCW78). If II Zw 70 is also seen close to edge-on, our observed rotation speed of 67 km s^{-1} within a $45''$ radius gives a dynamical mass of 8.3 billion M_{\odot} for this galaxy.

2.3. Line Profiles

A 21 cm line profile for this system was derived by summing the flux for each channel over the area containing line emission in the 21 cm total-intensity map of Figure 3. The 21 cm spectrum for the entire region is shown as a solid line in Figure 5. The total H I gas mass we derive for this system is $9 \times 10^8 M_{\odot}$, consistent with the results from BCW78 and (Richter *et al.* 1994). The 21 cm spectrum is very asymmetric, without the typical double-horned shape typical of spiral galaxies and other PRG's. This is not particularly surprising, however, as gas from the entire system is included, and the gas in the ring is not symmetric about the galaxy center.

As can be seen in Figure 3, it was impossible to distinguish the emission from II Zw 71 from that of the H I streamer in all of the velocity channels. We constructed approximate line profiles for each of the components by selecting regions for II Zw 70 and II Zw 71 in the total-intensity map and assuming that all emission in these regions belongs to these galaxies, and not to the streamer. The resulting global profiles for each component are shown as dashed lines in the figure. Because of the method we used in determining these profiles, the amount of gas belonging to II Zw 71 in the $1250\text{--}1300 \text{ km s}^{-1}$ velocity range is probably an overestimate, while in the same velocity range we underestimate the amount of gas in the H I streamer. Based upon these global profiles, we

estimate that 20% of the neutral hydrogen is associated with II Zw 70, 25% with the streamer, and the remaining 55% with the polar ring around II Zw 71. Based upon the use of a variety of different boxes for these regions, we estimate that the uncertainty introduced by our separation methods to be 10%.

For the dwarf galaxy II Zw 70, we derive $M_{\text{HI}}/L_B \simeq 0.3$. Though substantial, the H I mass of II Zw 71 is one of the smallest gas masses associated with known PRGs (*e.g.* (Richter *et al.* 1994); see Section 1). However, it is also rather small, and faint at optical wavelengths; so the ratio $M_{\text{HI}}/L_B \simeq 0.55$ is only slightly below the median for confirmed polar rings ((Sparke & Cox 2000)). These galaxies are both rather gas-rich, with values of M_{HI}/L_B typical of late-type spirals or gas-rich dwarf irregular galaxies (RH94; see Table 3). For the polar ring considered alone, $M_{\text{HI}}/L_B \simeq 2.4$, which is more typical of the blue low-surface-brightness disk galaxies in the sample of (Matthews & Gallagher 1997); see Figures 6 and 7.

3. Optical Observations

Optical images of the II Zw 70/71 system were obtained with the 1.8-meter Perkins telescope of the Ohio Wesleyan University and the Ohio State University at Lowell Observatory. We used the Ohio State University Imaging Fabry-Perot Spectrometer, without an etalon, as a focal-reducing camera. Observations were conducted on the night of 1995 April 8 through variable cirrus, and we obtained images totaling 5400 s in B , 1800 s in V , 2100 s in R , and 5400 s in a narrow-band $\text{H}\alpha$ filter. We observed again on the night of 1995 June 5 under photometric conditions and obtained shorter exposures in the same filters. The June images were calibrated using standards from Landolt (1983) and Barnes & Hayes (1982) and this calibration was transferred to our deeper April data using field stars. We produced a continuum-free $\text{H}\alpha$ image by scaling and subtracting the R image. Table 2 gives our derived magnitudes and colors.

In the B band image, and the $B - R$ color map of Figure 6, the polar ring appears very bumpy, with bright knots along it. There is also strong bending of the ring component, beginning fairly close to the central galaxy. The ring is also asymmetric, with the northern side brighter than the southern side. The close companion, II Zw 70, has irregular plumes extending from the main body at optical wavelengths. Our exposures were not deep enough to improve on the limit derived by BCW78 for an optical counterpart to the gas streamer.

The global colors of both galaxies are similar to those of late-type spiral galaxies (*e.g.*, RH94). The blue color of II Zw 71, however, is partly due to the light from the polar ring. We averaged in boxes over representative portions of the polar ring and the host galaxy (see Figure 6), and found $B - R \simeq 0.99$ for the host galaxy, while the ring is much bluer, with $B - R \simeq 0.65$ and $B - V \simeq 0.36$. The ring is significantly bluer than average for the disk of a late-type galaxy in the sample of de Jong (1995, 1996). However, both its color and its gas content are similar to the gas-rich low-surface-brightness disks of (Matthews & Gallagher 1997); the outer disks of the blue

low-surface-brightness galaxies of (Bell *et al.* 2000) also have similar optical colors.

The total V -band magnitude of II Zw 71 ($M_V = -17.3$) puts it about a magnitude below the mean Tully-Fisher relation defined by bright galaxies ((Pierce & Tully 1992)). However, II Zw 71 lies approximately on the Tully-Fisher relation for gas-rich extreme late-type galaxies ((Matthews *et al.* 1998b)), which have similar ratios of M_{HI}/L_B .

The continuum-subtracted $\text{H}\alpha$ image of II Zw 70 in Figure 6 shows ongoing star formation in the center. We also see filamentary $\text{H}\alpha$ emission in the southwestern plume, but not in the northeastern plume. Our measured line flux of 6.9×10^{-13} erg cm $^{-2}$ s $^{-1}$ yields a total energy output of 2.5×10^{40} erg s $^{-1}$ in $\text{H}\alpha$. Assuming that the initial mass function follows Salpeter’s form, we can use Kennicutt’s (1998) recipe to infer that II Zw 70 is producing $0.2M_{\odot}$ yr $^{-1}$ of new stars. At this rate, it would have taken $3 \times (M/L_B)$ Gyr to make the galaxy’s present population of stars, where M/L_B is the mass-to-light ratio in solar units. If the rate stays constant in the future, and we neglect gas recycled from aging stars, then the observed H I gas will be exhausted in 0.9 Gyr; this timescale is typical of starbursting irregulars ((Hunter 1997)).

The $\text{H}\alpha$ emission of II Zw 71 is from bright knots throughout the polar ring. The knot near the center could be either an H II region in the ring that is simply projected close to the center, or within the central galaxy itself. The ring emission is asymmetric. Even though the H I gas is more extended to the south, the northern half of the ring is much stronger in $\text{H}\alpha$, and is also the region where we detected the radio continuum emission shown in Figure 1. The measured $\text{H}\alpha$ flux of 1.2×10^{-13} erg cm $^{-2}$ s $^{-1}$ is significantly larger than that estimated by Reshetnikov & Combes (1994) from their slit spectrum. It translates to a total of 4.4×10^{39} erg s $^{-1}$ in $\text{H}\alpha$, corresponding to only $0.035M_{\odot}$ yr $^{-1}$ of new stars. Although the polar ring has almost the same colors as II Zw 70, it is making its stars much more slowly, at a pace more typical of irregular galaxies ((Hunter 1997)). At this rate, the observed H I gas would be consumed only over 14 Gyr, while it would have taken $6 \times (M/L_B)$ Gyr to make the ring’s present population of stars. However, Figure 3 of (Bell *et al.* 2000), using models in which star formation increases or decreases monotonically in time, shows that the ring’s observed blue color corresponds to a constant, or even rising, rate of starbirth. Thus despite its messy appearance, the ring in II Zw 71 is likely to be considerably older than the $\simeq 1$ Gyr suggested on morphological grounds by Reshetnikov & Combes.

4. Discussion: the Polar-Ring of II Zw 71

We observe H I gas in regular rotation about the minor axis of the optical polar ring in II Zw 71, and none that shares the rotation of the S0 disk. II Zw 71 is thus a confirmed polar-ring galaxy. The amount of H I is fairly modest, compared with other polar rings ((Richter *et al.* 1994)), but is much greater than normal for an S0 galaxy, and is more typical of a late-type spiral or large irregular galaxy ((Roberts & Haynes 1994)). As with other polar rings, the extent of the H I gas is greater than that of the optical ring. The rotation curve does not drop, even far outside the

optical radius of the host galaxy. As in other polar-ring galaxies, it appears that most of the mass in this galaxy is dark (*e.g.*, (Schweizer *et al.* 1983); (Whitmore *et al.* 1987); (Sackett *et al.* 1994); (Arnaboldi *et al.* 1997)).

The polar ring of II Zw 71 is asymmetric, at both optical and radio wavelengths. In addition, observations at H α show clumpy emission in the ring. This emission is more pronounced on the northern side of the galaxy, the same side on which faint, steep-spectrum radio continuum emission is observed. The presence of both H α emission and radio continuum emission along the ring, and its blue color, are strong arguments for ongoing star formation. The asymmetry of the ring material and the evidence of star formation in the ring make it likely that new material has recently been added to the polar ring, or that pre-existing ring material has recently been disturbed by a new interaction.

At our assumed distance of 18.1 Mpc, the projected separation of 4.4' between these two galaxies corresponds to a separation of $\simeq 23$ kpc. At a relative speed of 100 km s $^{-1}$, it would have taken these galaxies at least 230 Myr to separate after a close interaction. The orbital timescale for gas in the outer regions of II Zw 71 is about 200 Myr, implying that the most recent interaction between these two galaxies may have taken place within a few orbital timescales.

Was the polar ring of II Zw 71 formed by accretion from the companion galaxy II Zw 70? The two galaxies are smoothly connected in both position and velocity by a gaseous bridge or streamer, in which we observe no stellar component. Assuming that the bridge is the remnant of the interaction that created the polar ring, so that all of the gas from the polar ring and streamer originally belonged to II Zw 70, would yield $M_{\text{HI}}/L_{\text{B}} = 0.55$ prior to the interaction — a high, but not unreasonable, value for an irregular galaxy. Since the dynamical mass of II Zw 71 is more than twice that of II Zw 70, the outer layers of a gas-rich system the size of II Zw 70 would not have been very tightly bound, and might have been fairly easily detached.

The blue stars and H α regions in the polar ring are spread along a line, implying that much of the gas has already settled into a disk or ring, that we now see almost edge-on. It is difficult to explain how gas that was accreted only a few orbital timescales ago could have already settled into a plane. If there were enough dissipation to cause flattening on this short timescale, we would expect substantial amounts of accreted gas to be falling into the center of the host galaxy, and either forming stars there, or fueling a central black hole. However, this does not seem to be the case. Our observations reveal no radio continuum source, and the far-infrared IRAS flux is also low (PRC; (Richter *et al.* 1994)). The ionized gas of the central galaxy does not share the rotation axis of the ring material ((Reshetnikov & Combes 1994)), so it is unlikely to have come from the ring.

The contiguous streamer of gas between II Zw 70 and II Zw 71, as well as the star formation activity in both II Zw 70 and the polar ring, indicate an ongoing interaction between these two galaxies. However, the fact that HI gas to the east of the polar ring appears to be a continuation of the streamer to the west, in both position and velocity, implies that the streamer probably lies behind II Zw 71 or in front of it, rather than merging into the polar ring. That is not what we would

expect if both the polar ring and the streamer originated in the same, recent, accretion event. A further indication that the ring itself has existed for some time comes from the relatively weak $H\alpha$ emission. At the present rate of star formation, it would take several gigayears to build up the stars that we now observe in the ring, while the blue color indicates that starbirth was no more rapid in the past than it is now. We suggest instead that the polar ring of II Zw 71 predated the most recent close passage of II Zw 70, but was disturbed by it. Just as in the disks of spiral galaxies (Larson & Tinsley 1978, Mihos & Hernquist 1996, Barton, Geller & Kenyon 2000), tidal torques have ‘rejuvenated’ the ring, causing the vigorous star formation that we now observe.

ALC and LSS acknowledge support from the National Science Foundation through grant AST-9320403. The work reported here forms part of the PhD thesis of Andrea Cox, who was an NRAO Predoctoral Fellow while much of it was carried out. We would like to thank Michael Rupen and Jay Gallagher for helpful discussions.

REFERENCES

- Arnaboldi, M., Oosterloo, T., Combes, F., Freeman, K. C., & Koribalski, B. 1997, *AJ*, 113, 585
- Balkowski, C., Chamaraux, P., & Weliachew, L. 1978, *A&A*, 69, 263 (BCW78)
- Barnes, J. V., & Hayes, D. S. 1982, *The IRS Standard Star Manual* (Tucson: Kitt Peak National Observatory)
- Barton, E. J., Geller, M. J. & Kenyon, S. J. 2000, *ApJ*530, 660
- Bell, E. F., Barnaby, D., Bower, R. G., de Jong, R. S., Harper, D. A., Hereld, M., Loewenstein, R. F. & Rauscher, B. 2000, *MNRAS*, 312, 470
- Briggs, D. S. 1995, “High Fidelity Deconvolution of Moderately Resolved Sources”, *Ph.D. Thesis*, New Mexico Institute of Mining & Technology, March 1995
- Briggs, F. H., & Rao, S. 1993, *ApJ*, 417, 494
- Briggs, F. H. 1997, *ApJ*, 484, 29
- Brinks, E. 1993, in *The Cold Universe*, Th. Montmerle, Ch. J. Lada, I. F. Mirabel, & J. Trân Thanh Vân, Éditions Frontières, 303
- Carilli, C. L., & van Gorkom, J. H. 1992, *ApJ*, 399, 373
- Clarke, B. 1980, *A&A*, 89, 377
- Condon, J. J., Frayer, D. T., & Broderick, J. J. 1991, *AJ*, 101, 362
- Cornwell, T. J., Uson, J. M., & Haddad, N. 1992, *A&A*, 258, 583
- Cox, A. L. 1994, “A Step-by-Step Guide to Spectral-Line Data Analysis in AIPS”, Appendix B of *The AIPS Cookbook*, version 15-Jan-1996 (a publication of the National Radio Astronomy Observatory)
- Cox, A. L. 1996, Ph.D. Thesis, University of Wisconsin-Madison
- Cox, A. L., & Sparke, L. S. 1994, *BAAS* 195, 52.09
- Cox, A. L., Sparke, L. S., Richter, O.-G., & Shaw, M. 1994, in *Three-Dimensional Systems*, *Annals of the New York Academy of Sciences* Volume 751, edited by H. E. Kandrup, S. T. Gottesman, & J. R. Ipser (NYAS, New York), p. 751
- Cox, A. L., & Sparke, L. S., 1996, in *The Minnesota Lectures on Extragalactic Neutral Hydrogen*, *ASP Conf. Ser.* 106, edited by E. D. Skillman (ASP, San Francisco), p. 168
- Cox, A. L., Sparke, L. S., & van Moorsel, G. 2000, *in preparation*

- Dubinski, J., & Christodoulou, D. M. 1994, ApJ, 424, 615
- Galletta, G., Sage, L. J., & Sparke L. S. 1997, MNRAS, 284, 773
- van Gorkom, J. H., Schechter, P. L., & Kristian, J. 1987, ApJ, 314, 457
- Hagen-Thorn, V. A., & Reshetnikov, V. P. 1997, A&A, 319, 430
- Hibbard, J. E., & Mihos, J. C. 1995, AJ, 110, 140
- Hunter, D.A. 1997 PASP, 109, 937
- de Jong, R. S. 1996 A&A, 313, 377
- de Jong, R. S. 1995 PhD Thesis, Groningen University
- Kennicutt, R.C. 1998 ARA&A, 36, 189
- Kunth, D., Lequeux, J., Sargent, W. L. W., & Viallefond, F. 1994, A&A, 282, 709
- Landolt, A. U. 1983, AJ, 88, 853
- Larson, R. B. & Tinsley, B. M. 1978, ApJ, 315, 92
- Matthews, L. D. & Gallagher, J. S., III 1997, AJ, 114, 1899
- Matthews, L. D., van Driel, W., & Gallagher, J. S., III 1998a, AJ, 116, 1169
- Matthews, L. D., van Driel, W., & Gallagher, J. S., III 1998b, AJ, 116, 2196
- Mihos, J. C. & Hernquist, L. 1996, ApJ, 464, 641
- Pierce, M. J. & Tully, R. B. 1992, ApJ, 387, 47
- Reshetnikov, V. P., & Combes, F. 1994, A&A, 291, 57
- Richter, O.-G., Sackett, P. D., & Sparke, L. S. 1994, AJ, 107, 99
- Roberts, M. S., & Haynes, M. P. 1994, ARA&A, 32, 115 (RH94)
- Sackett, P. D., Rix, H.-W., Jarvis, B. J., & Freeman, K. C. 1994, ApJ, 436, 629
- Sackett, P. D. 1991, in *Warped Disks and Inclined Rings Around Galaxies*, S. Casertano, P. D. Sackett, & F. H. Briggs (Cambridge University Press), 73
- Schechter, P. L., Sancisi, R., van Woerden, H., & Lynds, C. R. 1984, MNRAS, 208, 111
- Schweizer, F., Whitmore, B. C., & Rubin, V. C. 1983, AJ, 88, 909
- Sparke, L. S. 1996, ApJ, 473, 810

Sparke, L.S. & Cox, A.L. 2000 in *XVth IAP meeting: Dynamics of Galaxies*, ASP Conf. Ser. 192 (ASP: San Francisco), p119

Taylor, C. L., Thomas, D. L., Brinks, E., & Skillman, E. D. 1996, *ApJS*, 107, 143

Whitmore, B. C., McElroy, D. B., & Schweizer, F. 1987, *ApJ*, 314, 439

Whitmore, B. C., Lucas, R. A., McElroy, D.B., Steiman-Cameron, T. Y., Sackett, P. D., & Olling, R. P. 1990, *AJ*, 100, 1489 (PRC)

Whitmore, B. C. 1991 in *Warped Disks and Inclined Rings Around Galaxies*, S. Casertano, P. D. Sackett, & F. H. Briggs (Cambridge University Press), 60

Zwaan, M. A., Briggs, F. H., Sprayberry, D., & Sorar, E. 1997, *ApJ*, 490, 173

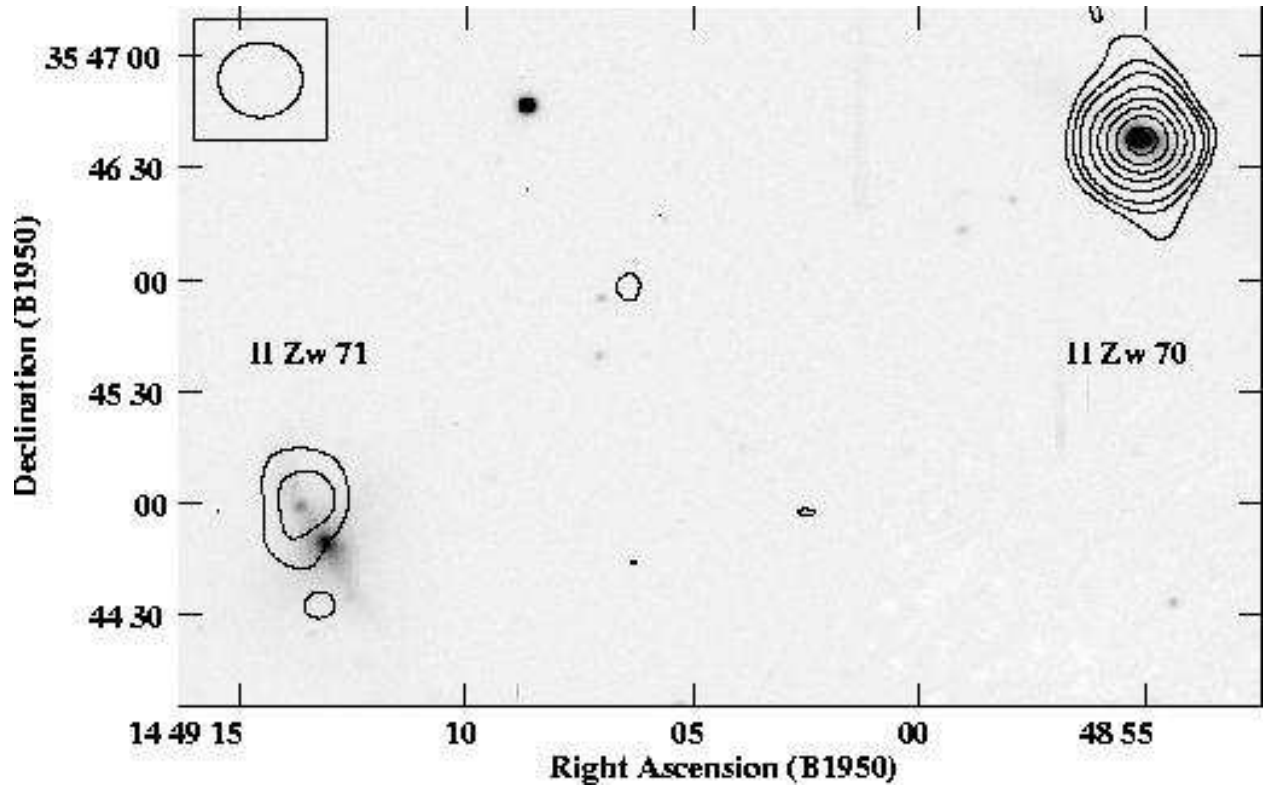


Fig. 1.— 21 cm radio continuum contours for the II Zw 71/70 system, overlaid on the optical (B band) image taken with the Ohio State University Imaging Fabry-Perot Spectrometer (IFPS). The continuum map was constructed from an average of the line-free channels. II Zw 71 (on the left) is the candidate polar-ring galaxy, and II Zw 70 (right) is the dwarf companion. The peak flux is $4.5 \text{ mJy beam}^{-1}$, and the solid contour levels are at 3, 4.5, 6, 9, 12, 15, & $18\text{-}\sigma$, where $\sigma = 0.2 \text{ mJy beam}^{-1}$.

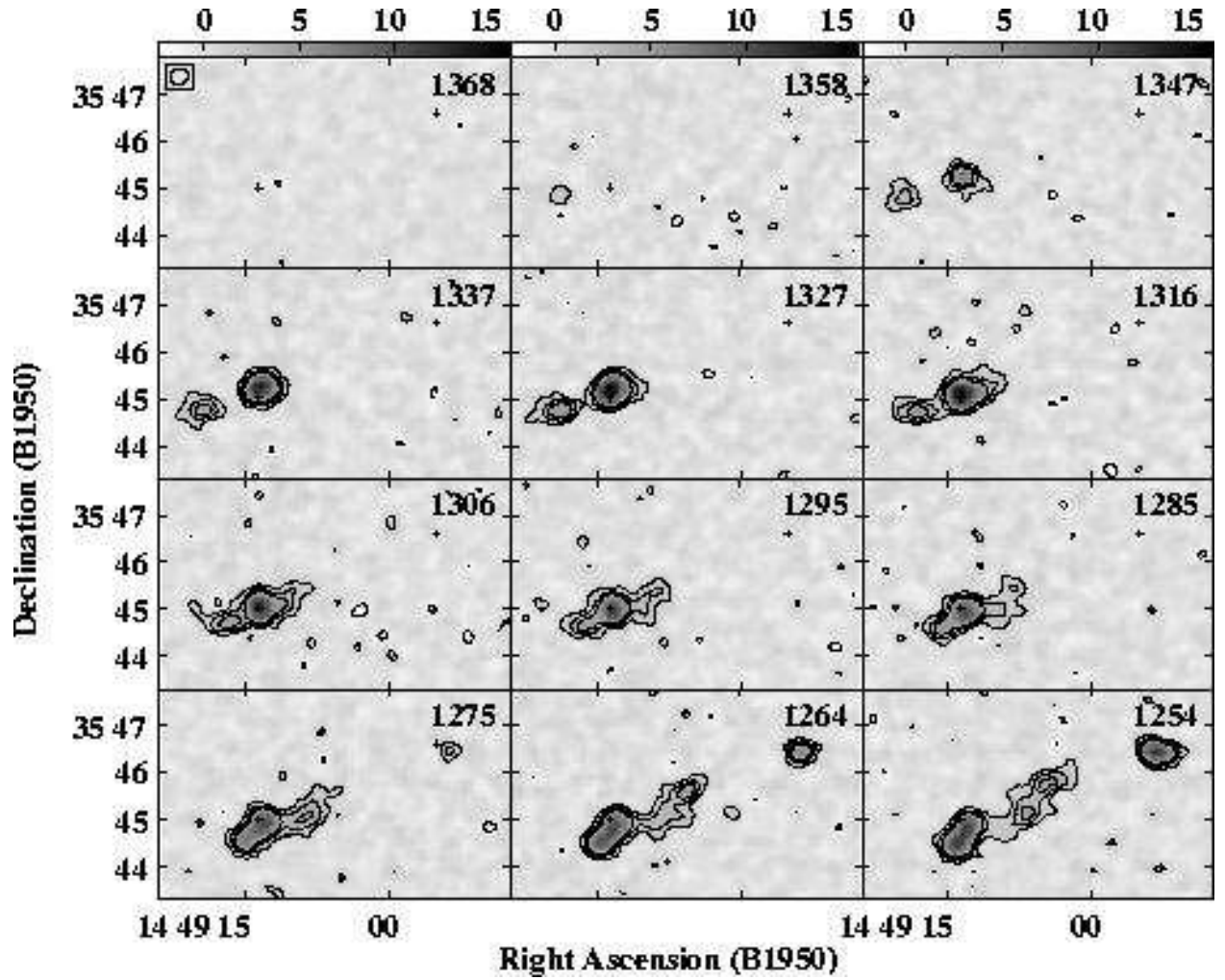
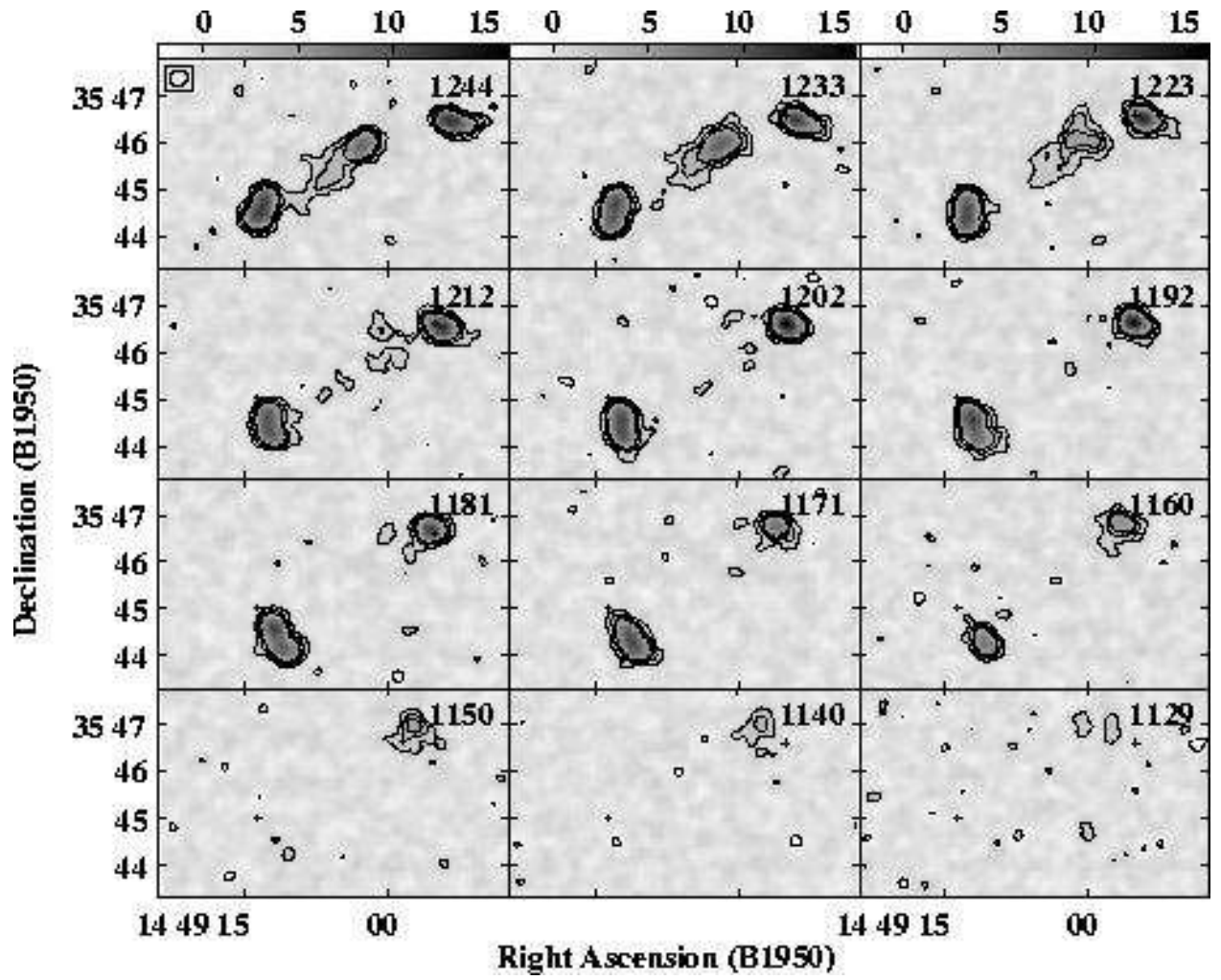


Fig. 2.— 21 cm channel maps for the II Zw 71/70 system, smoothed to 10 km s^{-1} velocity resolution. The crosses mark the central positions of II Zw 71 (east) and II Zw 70 (west). The synthesized beam is shown in the upper left-hand corner of the first channel, and each channel is labelled with its central velocity in km s^{-1} . Dashed contours are at -3σ ; solid contours are at $3, 6, \& 9\sigma$ ($\sigma = 0.4 \text{ mJy beam}^{-1}$). The greyscale levels are shown (in mJy) at the top of the image.



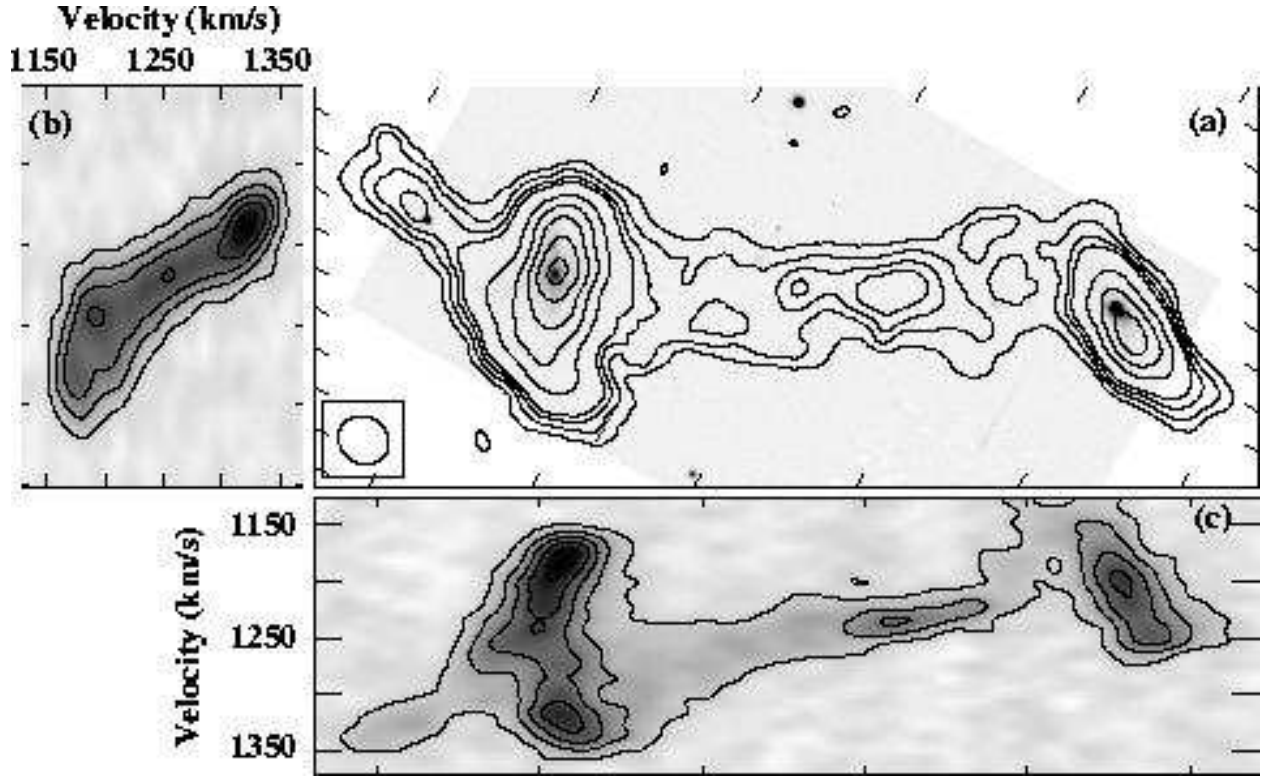


Fig. 3.— (a) Total-H I contours superposed on the optical (B band) image of Figure 1. Shown are II Zw 71 (east), II Zw 70 (west), and the H I cloud between the two objects. The image has been rotated 30° so that the apparent major axis of the gaseous cloud is horizontal. Notice the extension of the streamer on the eastern side of II Zw 71 (the unresolved optical source at that location is a star). The 21 cm synthesized beam is shown in the lower left corner. (b) Position-velocity cut along the apparent major axis of the optical polar ring. This cut is a single $5''$ pixel wide. (c) Position-velocity sum along the apparent major axis of the gaseous cloud. The sum includes all 21 cm line emission detected from the streamer (see Section 2.2).

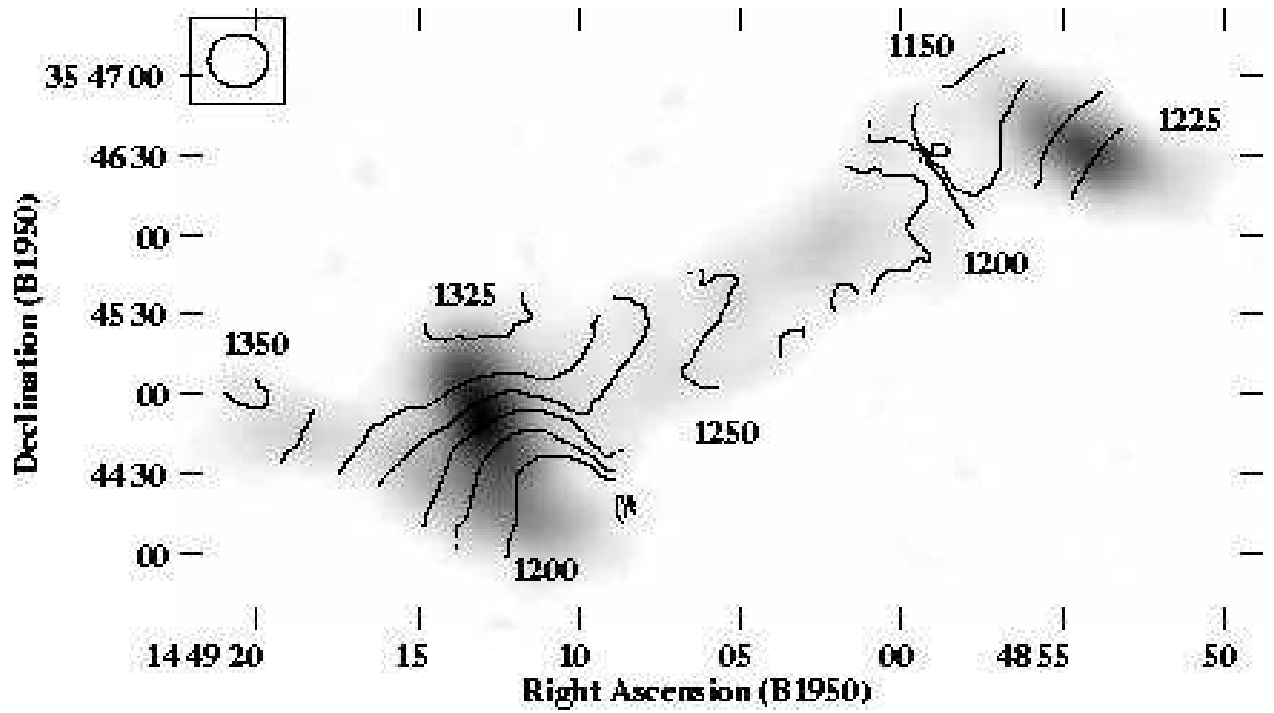


Fig. 4.— Intensity-weighted velocity field (contours) of the II Zw 70/71 system, overlaid on the total-H I map (greyscale) of Figure 3. Contour labels are in km s^{-1} , and all contours are separated by 25 km s^{-1} . The 21 cm synthesized beam is shown in the upper left corner.

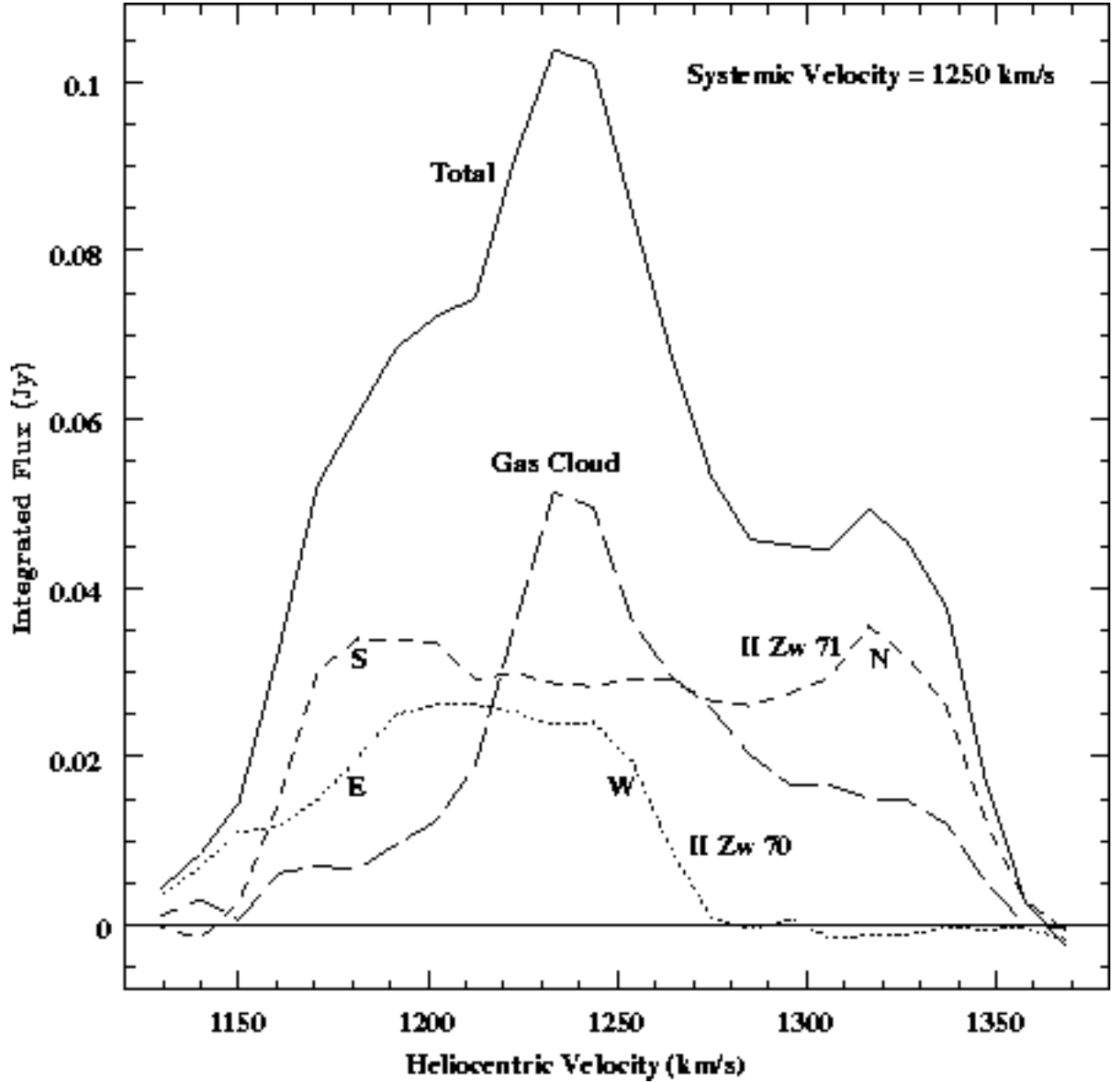


Fig. 5.— 21 cm line profile for the II Zw 71/70 system. The solid line includes emission from the entire system, and the dashed lines show emission from each component, as labeled. The high-velocity and low-velocity ends of the line profiles for II Zw 70 and II Zw 71 are labeled to make it clear which part of each galaxy corresponds to these velocities. The velocity width of the entire system at 20% power is $\simeq 300 \text{ km s}^{-1}$, and the redshift of the system, determined from the midpoint of this range, is 1250 km s^{-1} .

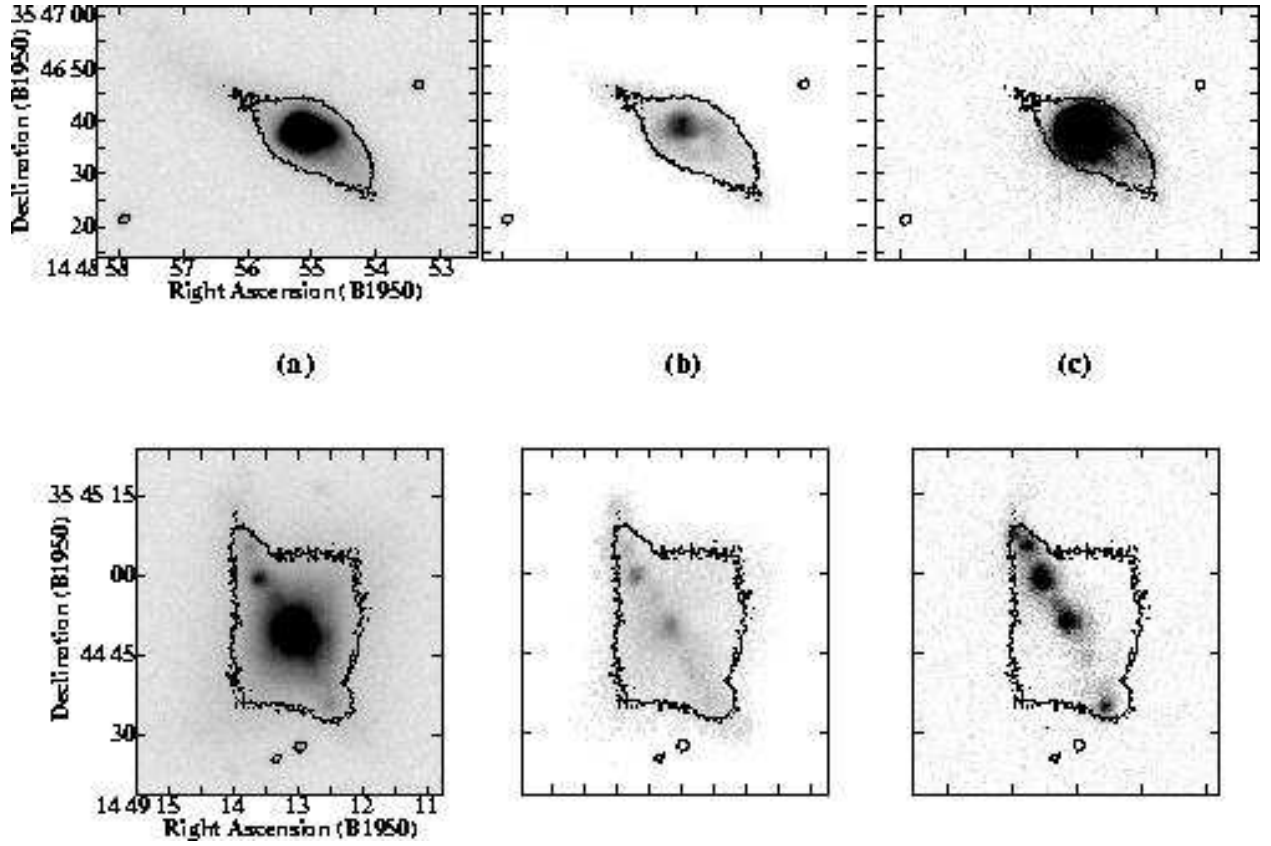


Fig. 6.— Optical images of II Zw 70 (top) and II Zw 71 (bottom). All images are to the same spatial scale. (a) R band images. (b) B-R color maps of II Zw 70 (top) and II Zw 71 (bottom). The contour represents the lowest R band contour from (a). Darker regions are bluer. (c) H α images. The contour represents the lowest R band contour from (a).

Table 1. Instrumental Parameters: 21cm Observations of II Zw 70

Parameter	II Zw 70	
	C	D
Array configuration	C	D
Observing dates	02 Dec 1994	02 May 1995
Time on-source (hr)	5.72	3.22
Number of antennas ^a	26	26
Shortest, longest baseline (m)	73, 3400	35, 1030
Field center (1950) ^b	$14^h 49^m 03^s$ $+35^\circ 45' 42''$	
Velocity of band center, heliocentric (km s ⁻¹) ^c	IF 1	1268
	IF 2	1232
Number of velocity channels ^d	128	
Frequency channel spacing (kHz) ^d	12.2	
Velocity channel spacing (km s ⁻¹) ^d	2.6	
Final velocity of band center, (km s ⁻¹) ^d	1247	
Final number of velocity channels ^d	49	
Final velocity channel spacing, (km s ⁻¹) ^e	5.2	
FWHP of synthesized beam(") ^d	22.5×20	
RMS noise in channel maps (mJy beam ⁻¹) ^d	0.4	

^a Only 26 of the VLA’s 27 antennas were used for these observations, as one antenna was allocated for VLBI observations.

^b This parameter was the same for all observations of this galaxy.

^c This galaxy was observed with two offset bandpasses (IF’s). All parameters other than the central velocity were identical for these IF’s. The final maps were produced by combining data from both bandpasses.

^d The numbers quoted here are for the final maps after combining the data from both arrays and both IF’s. The edges of the two bandpasses were cropped to eliminate the noisy end-channels, and the remaining data were combined to make a single dataset with a wide enough bandwidth to contain the velocity range of both galaxies.

^e The final maps were smoothed to 5.2 km s⁻¹ velocity resolution. The high velocity resolution of the original observations was necessary for an independent project by E. Brinks involving the same galaxy pair.

Table 2. Optical magnitudes & colors in the II Zw 70/71 system

Quantity ^a	II Zw 70	II Zw 71	Component	
			host galaxy	polar ring
m_B	14.78	14.42	$\simeq 14.7^b$...
m_V	14.45	13.99
m_R	14.23	13.59
B-V			0.56	0.36
B-R			0.99	0.65
V-R			0.43	0.30
M_B	-16.5	-16.9	$\simeq -16.6$...
$L_B (L_\odot)$	6.2×10^8	8.7×10^8	$\simeq 6.7 \times 10^8$...

^a No extinction corrections were made to the optical magnitudes to account for the orientation of the galaxies.

^b An approximate B magnitude for the host galaxy only was calculated by subtracting off the brightest parts of the polar ring from the B band image using a scaled version of the H-alpha line image.

Table 3. Physical Parameters for the II Zw 70/71 system

PARAMETER	Source Name		
	II Zw 70	II Zw 71	streamer
UGC number	UGC 9560	UGC 9562	—
Position (B1950)	$\alpha =$	$14^h 49^m 13^s$	$14^h 48^m 55^s.1$
	$\delta =$	$+35^\circ 44' 47''$	$+35^\circ 46' 37''$
21 cm Redshift (km s^{-1}) ^a	1195	1250	1200 - 1345
Rotation speed (km s^{-1}) ^b	67	95	...
Angular diameter at 21cm	$\simeq 90''$	$\simeq 100''$...
H I line integral (Jy km s^{-1}) ^c	2.6	6.2	3.2
Systemic velocity (km s^{-1}) ^d	1310	1366	...
Distance (h^{-1} Mpc) ^e	13.6	13.6	13.6
Linear radius in H I (h^{-1} kpc)	3.0	3.3	...
M_{HI} ($h^{-2} M_\odot$) ^c	1.0×10^8	$\simeq 2.7 \times 10^8$	$\simeq 1.4 \times 10^8$
Total Mass, M_{dyn} ($h^{-1} M_\odot$)	6.2×10^9	14×10^9	...
$M_{\text{HI}}/M_{\text{dyn}}$ (h^{-1})	0.02	0.02	...
M_{HI}/L_B	0.32	0.55 ^f	...

^a Midpoint between the 20% level of the 21 cm profile.

^b Half-width of the 21 cm line at 20% power

^c The 21cm line integrals and H I masses listed here are based upon the line profiles shown in Figure 5. The method used to estimate the amount of emission associated with each object is described in Section 2.3.

^d After correcting for solar motion of 300 km s^{-1} towards $l = 90^\circ$, $b = 0^\circ$.

^e All distance-related parameters are written in terms of the dimensionless unit $h = H_0/100 \text{ km s}^{-1} \text{ Mpc}$. The systemic velocity assumed for the system is 1364 km s^{-1} , and the same distance is used for all three components of the II Zw 70/II Zw 71/streamer system. (The systemic velocity is based upon a redshift of 1249 km s^{-1} , which is the midpoint at 20% power of the global line profile in Figure 5.)